




# Micropillar compression testing of powders

Emily L. Huskins<sup>1,4</sup> · Zachary C. Cordero<sup>2</sup> · Christopher A. Schuh<sup>2</sup> · Brian E. Schuster<sup>3</sup> 

Received: 12 May 2015 / Accepted: 11 July 2015 / Published online: 21 July 2015  
© Springer Science+Business Media New York (outside the USA) 2015

**Abstract** An experimental design for microcompression on individual powder particles is proposed as a means of testing novel materials without the challenges associated with consolidation to produce bulk specimens. This framework is demonstrated on an amorphous tungsten alloy powder, and yields reproducible measurements of the yield strength ( $4.5 \pm 0.3$  GPa) and observations of the deformation mode (in this case, serrated flow by shear localization).

## Introduction

Microcompression testing is a powerful tool for characterizing materials that are not amenable to standard macrocompression testing, such as nanocrystalline and nanolaminate thin films [1–5], high pressure torsion specimens [6–9], and phase-specific tests in multi-phase alloys [10–14]. In this technique, micron- or submicron-scale pillars are compressed in a nanoindenter fitted with a flat punch tip. Such tests are often coupled with post-mortem

imaging of the pillars to identify the pillars' deformation mode [15, 16].

Early applications of microcompression focused on the study of size effects, by which a material's measured strength increases with decreasing sample diameter [15]. Typically, size effects have been attributed to a change in deformation mode as the characteristic sample length scale approaches that of the microstructural features that control plastic flow. Conversely, it is also possible to obtain mechanical properties comparable to those of bulk compression tests by designing specimens that are sufficiently larger than the characteristic length scale of the dominant microstructural features [16–23]. For amorphous metals, these microstructural features are near the atomic scale, which is at least an order of magnitude smaller than a typical pillar diameter of several microns. Thus, microcompression experimentation on submicron amorphous pillars generally conforms to expected behavior of bulk materials with identical microstructures [24–26].

Amorphous metals can be produced through a variety of powder processing techniques where the resulting powder particles are on the order of dozens of microns, but it is very challenging to produce bulk specimens from such powders without introducing flaws that affect the bulk properties. Thus, the ability to perform microcompression experiments on the powder particles directly would provide two benefits. (1) The inherent mechanical properties of the material could be obtained in the absence of extrinsic effects of microstructural features introduced during consolidation (such as porosity, devitrification, oxide incorporation, etc.) which may dominate the mechanical behavior of bulk samples. (2) During the powder-route synthesis of new alloys with non-equilibrium microstructures, one could rapidly identify powders with attractive mechanical properties before investing the time and

✉ Brian E. Schuster  
brian.e.schuster.civ@mail.mil

<sup>1</sup> Oak Ridge Institute for Science and Education Postdoctoral Fellowship Program, Army Research Laboratory, Aberdeen Proving Ground, MD 21005, USA

<sup>2</sup> Department of Materials Science and Engineering, MIT, Cambridge, MA 02139, USA

<sup>3</sup> RDRL-WML-H, Weapons and Materials Research Directorate, Army Research Laboratory, Aberdeen Proving Ground, MD 21005, USA

<sup>4</sup> Present Address: Mechanical Engineering Department, United States Naval Academy, Annapolis, MD 21402, USA

resources to address the challenge of consolidation. The challenge, then, is to develop an experimental regimen that will produce a valid micromechanical test on specimens produced from individual powder particles.

This work describes the application of microcompression testing to an amorphous tungsten alloy powder possessing interesting mechanical properties [27]. By accounting for substrate effects and combining mechanical tests with post-mortem microscopy, the powder particles' yield strengths and their deformation modes were successfully measured.

## Experimental methods

Amorphous alloy powders were prepared by mechanically alloying nominally pure W with 27 wt% Co (99.95 % W, –200 + 325 mesh; 99.8 % Co, –100 + 325 mesh) and 4 wt% stearic acid for 60 h in a SPEX 8000 high-energy ball mill using a hardened steel vial and media, and a ball-to-powder ratio of 5:1 (10 g of powder). Milling was performed under an ultrahigh-purity Ar atmosphere in a glovebox to avoid oxidation. The composition of the as-milled amorphous powder was W–38Co–9Fe–20C, at.% according to a previous study [27]. The as-milled powder's particle size distribution was measured using a Horiba LA-950V2 laser diffraction particle size analyzer.

The structure of the as-milled powder was characterized using transmission electron microscopy (TEM) and X-ray diffraction (XRD). TEM samples were prepared by mounting the powders in epoxy, grinding the powder/epoxy disks to a thickness of roughly 15  $\mu\text{m}$ , and then Ar ion polishing the disks to electron transparency in a Fischione 1010 ion mill. During ion polishing, the samples were cooled to 150 K using a liquid nitrogen cold finger. The samples were imaged in a JEOL 2010F TEM operated at 200 kV. XRD patterns were collected on a PANALYTICAL X'Pert Pro using Cu K $\alpha$  radiation.

The as-milled powders were cold-pressed into a 1-cm-diameter green compact under a uniaxial pressure of 500 MPa. This green compact was mounted in epoxy (Struers, Epofix), and then mechanically ground and polished, with a final polishing step of colloidal silica. Pillars were ion-milled out of individual cross-sectioned powder particles. The pillar diameters were such that the epoxy would remain elastic during the microcompression test, and selected by approximating the particle as a rigid, spherical punch pushing into a conforming cavity in a semi-infinite substrate (in this case the epoxy matrix). Under this approximation, the substrate should remain elastic as long as the following relationship holds:

$$0.91 \left( \frac{D_{\text{Pillar}}}{D} \right)^2 \sigma_{\text{Pillar}} < \sigma_{\text{Sub}}, \quad (1)$$

where  $D_{\text{Pillar}}$  is the micropillar's diameter,  $D$  the diameter of the particle,  $\sigma_{\text{Sub}}$  the uniaxial, compressive yield strength of the substrate, and  $\sigma_{\text{Pillar}}$  is the yield strength of the pillar. Equation 1 is derived by equating the load required to yield the pillar (uniaxial compressive yield) with the load needed to yield the epoxy substrate (multi-axial contact yield), following [28, 29]. Realistically, particles may be in contact within the green compacts, including below the surface. These neighboring particles will help bear some of the load. Equation 1 is therefore considered a lower bound estimate in which neighbor particles are significantly far away. Elastic deformation in the substrate, however, does contribute to the total displacement measured by the nanoindenter. The calculated engineering strain will be larger as a result of this added compliance. This makes it difficult to accurately measure the Young's modulus of the powder particles with this technique [30]. The engineering stress measurements are unaffected by the substrate's elastic deformation and are still valid.

Uniaxial compression tests on the epoxy gave a Young's modulus of 1.4 GPa and a yield strength of  $44 \pm 1$  MPa. Preliminary indentation and microcompression tests suggested  $\sigma_{\text{Pillar}} \sim 5$  GPa. Substitution of these values into Eq. 1 suggests the epoxy substrate would remain elastic for pillars smaller than 2.5  $\mu\text{m}$  in diameter fabricated from particles larger than  $\sim 25$   $\mu\text{m}$  in diameter. Reduction of the pillar diameter or an increased particle diameter would imply an additional safety factor on maintaining an elastic response in the epoxy substrate. In light of this calculation, cylindrical and tapered micropillars with diameters of 2.4  $\mu\text{m}$  and aspect ratios of 2–3 were ion-milled out of cross-sectioned particles larger than 40  $\mu\text{m}$  in a FEI Nova Nanolab 600i dual-beam focused ion beam. The cylindrical samples were milled using the lathe technique [31], and an example of a cylindrical micropillar milled out of a single powder particle is shown in Fig. 1. The tapered pillars had an average taper angle of 2.5°, and the engineering stress was calculated using the cross-sectional area at the top of the pillar.

The microcompression experiments were performed in an MTS Nanoindenter XP with a square,  $30 \times 30$   $\mu\text{m}$  flat punch diamond tip. Tests were conducted under load control set to provide a nominal strain rate of  $10^{-3}$   $\text{s}^{-1}$ . Following the tests, the pillars were inspected in the dual-beam microscope to identify their deformation and failure modes.

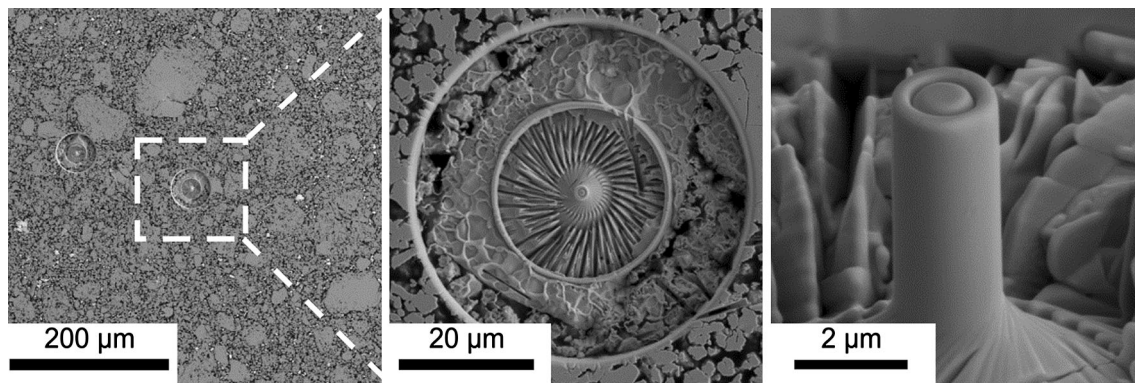


**Fig. 1** SEM micrographs of a lathe-milled micropillar fabricated from an amorphous WCoFeC powder particle mounted in epoxy. *Dark regions* are the epoxy, *light regions* the amorphous material

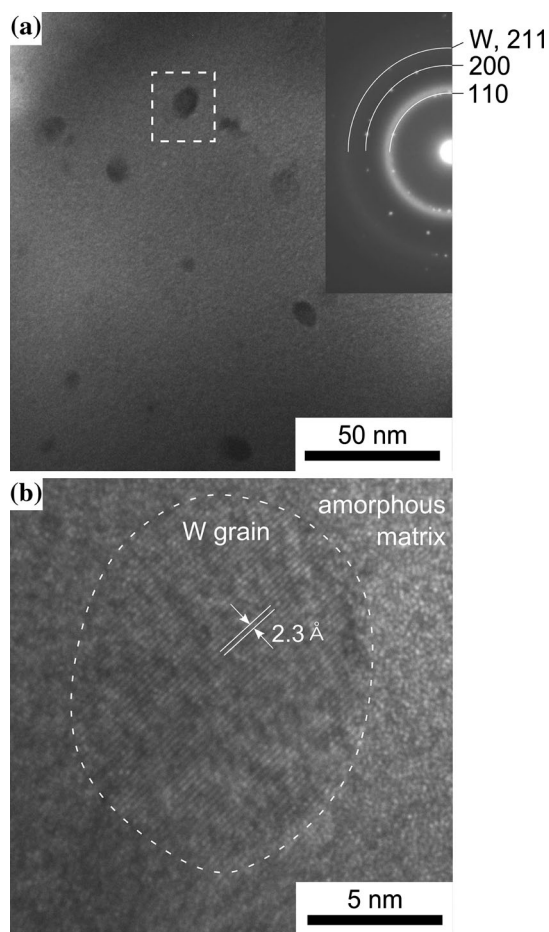


**Fig. 2** **a** TEM micrograph of the amorphous powder containing a small volume fraction of residual crystalline W nanograins (*darker contrast*). **b** High-resolution TEM micrograph of the *boxed region* in **a** showing lattice fringes of a nanograin. These lattice fringes have a 2.3 Å wavelength that corresponds to the W 110 *d*-spacing, 2.2 Å

### Powder microstructure and particle size distribution

The TEM micrographs of the amorphous powder in Fig. 2a, b show that these powders were predominantly amorphous with a small volume fraction of a residual crystalline phase. This interpretation is supported by the SAD pattern inset in Fig. 2a, which features the diffuse halos characteristic of an amorphous metal overlaid with crystalline diffraction spots. The crystalline phase was identified as residual, unmixed W from the XRD pattern. The volume-average, circular-equivalent diameter of these tungsten nanograins was 6 nm, and assuming a TEM sample thickness of 50 nm, their total volume fraction was <math><0.01</math> and their mean separation was 900 nm [32]. Our powder's microstructure is nearly identical to that of the powders described in Ref. [27].

The powder's particle size distribution is shown in Fig. 3 along with log-normal fits to the data. The particles had a volume-average diameter of  $\sim 10 \mu\text{m}$  which is in line with previous reports on the high-energy ball milling of metals that do not cold weld [33].

### Results and discussion

Figure 4 contains representative stress–strain curves from microcompression tests on these cylindrical pillars alongside micrographs of the pillars after testing. The average 0.2 % offset yield strength of these pillars was  $4.5 \pm 0.3 \text{ GPa}$ , which is exceptionally high [34]. This high strength is due to the fact that the strength of an amorphous metal is directly proportional to the shear modulus of the

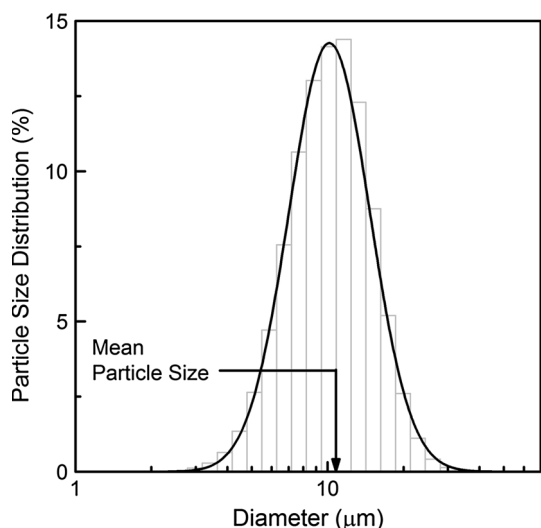


**Fig. 3** Particle size distribution of the amorphous WCoFeC powders along with a log-normal fit to the data

base metal, and this particular alloy’s base metal is tungsten, which has one of the highest shear moduli of the transition metals [35]. The 0.3 GPa variation in this yield strength is in line with that of other metallic glass micropillars with similar diameters, and can be attributed to the pillars’ variable atomic scale structure [24]. The apparent hardening seen in the stress–strain curves in Fig. 4 is an artifact of plotting engineering stress values which do not account for the increase in pillar-platen contact area after the pillars start to yield. Load–unload–reload experimental results, not shown here, confirm that the flow stress at yield, unloading, and reloading, as calculated using their corresponding pillar diameters, does not show hardening behavior, as expected for an amorphous metal.

All of the stress–strain curves shown in Fig. 4 exhibit the intermittent flow commonly observed during the microcompression testing of amorphous metals [24–26, 36–40]. The shear offsets seen on the pillars’ surfaces in

the accompanying micrographs suggest that the pop-ins in these stress–strain curves correspond to shear banding events. That these pillars deform by shear localization is consistent with past reports on the microcompression testing of metallic glass pillars with diameters >1 μm [41–44]. In most tests, only a single pop-in was observed, followed by pillar failure but occasionally tests captured multiple pop-in events, separated by regions of continued elastic deformation.

Figure 5 contains engineering stress–strain curves from microcompression tests performed on tapered pillars as well as micrographs of the as-tested pillars. These tapered pillars were useful because, in comparison with the cylindrical pillars, they generally supported more shear banding events prior to fracturing, as has been observed by others [45]. This made it easier to stop the microcompression test beyond the first yield point but before failure. The intermittent flow in these stress–strain curves and the shear offsets seen on the pillars’ surfaces demonstrate that the deformation mode is unaffected by the taper; the pillars still deform by shear localization. Including the taper did however increase the average yield strength by 25 % to  $5.7 \pm 0.2$  GPa. This 25 % increase in the yield strength aligns well with predictions by Schuster et al. [26], who argued that tapering can artificially increase an amorphous metal’s strength because, in a tapered pillar, higher loads are necessary to exceed the yield strength along the entire shear path. Inspection of the pillars’ surfaces revealed a near one-to-one correspondence between the number of shear offsets and serrations in the stress–strain curve. Occasional differences between these values suggest that, e.g., multiple shear bands nucleated during a single pop-in or the same shear band was re-activated in separable events.

The most notable result from these experiments is this amorphous powder’s exceptionally high yield strength. In light of other studies on taper-free metallic glass pillars with similar dimensions, this yield strength would likely

**Fig. 4** Engineering stress–strain curves from a microcompression tests on cylindrical, taper-free pillars ion-milled out of amorphous WCoFeC powder particles. The accompanying inset micrographs are of the as-tested pillars. Pop-in events are clearly observed in the first experiment. All samples show evidence of shear localization

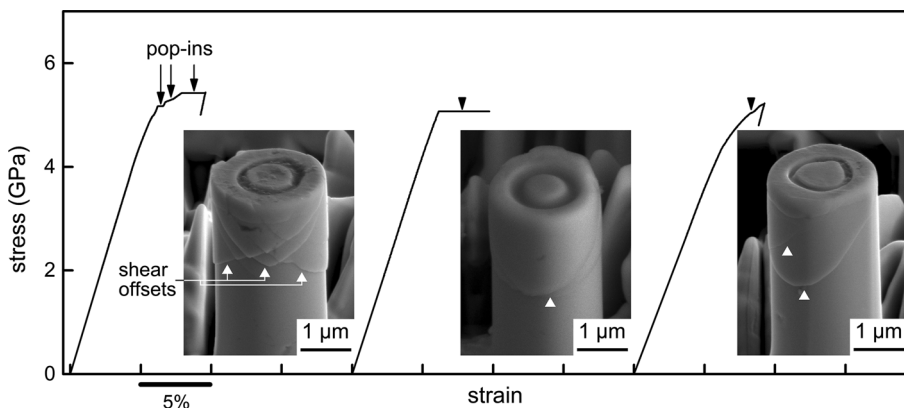
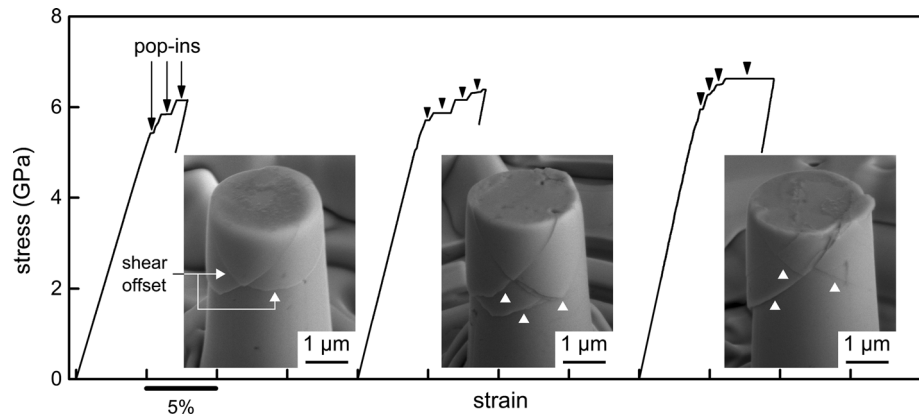


**Fig. 5** Engineering stress–strain curves from microcompression tests performed on tapered pillars with corresponding post-deformation micrographs



match that of bulk specimens if such specimens could be prepared [25, 26, 44]. The other phenomena seen in these microcompression tests are consistent with prior studies on the microcompression testing of metallic glasses, confirming that microcompression testing of powder particles can be used to extract a powder's intrinsic deformation behavior.

## Conclusions

In this work, a microcompression experimental technique for testing individual powder particles was applied to a powder processed amorphous tungsten-based alloy with a non-equilibrium microstructure. The substrate effects on the measured strength were mitigated by an appropriate choice of pillar diameter related to particle size. The material's yield strength was found to be exceptionally high at  $\sim 4.5$  GPa and pop-in events in the engineering stress–strain curves were observed, suggesting deformation occurs through shear localization. Post-mortem microscopy revealed evidence of shear offsets, confirming this conclusion. The described experimental technique can be used to identify intrinsic mechanical properties, absent of extrinsic effects commonly observed during bulk testing as a result of defect introduction during consolidation. An ideal bulk material sharing the same microstructure would be expected to share the same intrinsic mechanical properties.

**Acknowledgements** This study was supported by the US Defense Threat Reduction Agency under Grant No. HDTRA1-11-1-0062. ELH acknowledges support through the Oak Ridge Institute for Space and Education (ORISE) Program #1120-1120-99. ZCC gratefully acknowledges support from the Department of Defense through the NDSEG fellowship program. BES would like to acknowledge support work from the Cooperative Research and Development Agreement #11-24.

## References

- Khalajhedayati A, Rupert TJ (2014) Emergence of localized plasticity and failure through shear banding during microcompression of a nanocrystalline alloy. *Acta Mater* 65:326–337
- Schuster BE, Wei Q, Zhang H, Ramesh KT (2006) Microcompression of nanocrystalline nickel. *Appl Phys Lett* 88: 103112–103113
- Gu XW, Loynachan CN, Wu Z et al (2012) Size-dependent deformation of nanocrystalline Pt nanopillars. *Nano Lett* 12: 6385–6392
- Jang D, Greer JR (2011) Size-induced weakening and grain boundary-assisted deformation in 60 nm grained Ni nanopillars. *Scr Mater* 64:77–80
- Mara NA, Bhattacharyya D, Hirth JP et al (2010) Mechanism for shear banding in nanolayered composites. *Appl Phys Lett* 97:021909
- Nagoshi T, Shibata A, Todaka Y et al (2014) Mechanical behavior of a micro-sized pillar fabricated from ultrafine-grained ferrite evaluated by a microcompression test. *Acta Mater* 73:12–18
- Ligda JP, Schuster BE, Wei Q (2012) Transition in the deformation mode of nanocrystalline tantalum processed by high-pressure torsion. *Scr Mater* 67:253–256
- Wei Q, Pan ZL, Wu XL et al (2011) Microstructure and mechanical properties at different length scales and strain rates of nanocrystalline tantalum produced by high-pressure torsion. *Acta Mater* 59:2423–2436
- Edalati K, Toh S, Iwaoka H et al (2012) Ultrahigh strength and high plasticity in TiAl intermetallics with bimodal grain structure and nanotwins. *Scr Mater* 67:814–817
- Williams JJ, Walters JL, Wang MY et al (2013) Extracting constitutive stress–strain behavior of microscopic phases by micropillar compression. *JOM* 65:226–233
- Stewart JL, Jiang L, Williams JJ, Chawla N (2012) Prediction of bulk tensile behavior of dual phase stainless steels using constituent behavior from micropillar compression experiments. *Mater Sci Eng A* 534:220–227
- Ghassemi-Armaki H, Maaß R, Bhat SP et al (2014) Deformation response of ferrite and martensite in a dual-phase steel. *Acta Mater* 62:197–211
- Okamoto NL, Kashioka D, Inomoto M et al (2013) Compression deformability of  $\Gamma$  and  $\zeta$  Fe–Zn intermetallics to mitigate detachment of brittle intermetallic coating of galvanized steels. *Scr Mater* 69:307–310

14. Wheeler JM, Raghavan R, Chawla V et al (2014) Deformation of hard coatings at elevated temperatures. *Surf Coat Technol* 254:382–387
15. Greer JR, Oliver WC, Nix WD (2005) Size dependence of mechanical properties of gold at the micron scale in the absence of strain gradients. *Acta Mater* 53:1821–1830
16. Uchic MD, Dimiduk DM, Florando JN, Nix WD (2004) Sample dimensions influence strength and crystal plasticity. *Science* 305:986–989
17. Porter WJ, Uchic MD, John R, Barnas NB (2009) Compression property determination of a gamma titanium aluminide alloy using micro-specimens. *Scr Mater* 61:678–681
18. Girault B, Schneider AS, Frick CP, Arzt E (2010) Strength effects in micropillars of a dispersion strengthened superalloy. *Adv Eng Mater* 12:385–388
19. Kiener D, Hosemann P, Maloy SA, Minor AM (2011) In situ nanocompression testing of irradiated copper. *Nat Mater* 10:608–613
20. Gu R, Ngan AHW (2013) Size effect on the deformation behavior of duralumin micropillars. *Scr Mater* 68:861–864
21. Dimiduk DM, Uchic MD, Rao SI et al (2007) Overview of experiments on microcrystal plasticity in FCC-derivative materials: selected challenges for modelling and simulation of plasticity. *Model Simul Mater Sci Eng* 15:135
22. Shade PA, Uchic MD, Dimiduk DM et al (2012) Size-affected single-slip behavior of René N5 microcrystals. *Mater Sci Eng A* 535:53–61
23. Pouchon MA, Chen J, Ghisleni R et al (2008) Characterization of irradiation damage of ferritic ODS alloys with advanced micro-sample methods. *Exp Mech* 50:79–84
24. Schuster BE, Wei Q, Ervin MH et al (2007) Bulk and microscale compressive properties of a Pd-based metallic glass. *Scr Mater* 57:517–520
25. Volkert CA, Donohue A, Spaepen F (2008) Effect of sample size on deformation in amorphous metals. *J Appl Phys* 103:083539–083539-6. doi:10.1063/1.2884584
26. Schuster BE, Wei Q, Hufnagel TC, Ramesh KT (2008) Size-independent strength and deformation mode in compression of a Pd-based metallic glass. *Acta Mater* 56:5091–5100
27. Cho K, Schuh CA (2015) W-based amorphous phase stable to high temperatures. *Acta Mater* 85:331–342
28. Field JS, Swain MV (1993) A simple predictive model for spherical indentation. *J Mater Res* 8:297–306
29. Francis HA (1976) Phenomenological analysis of plastic spherical indentation. *J Eng Mater Technol* 98:272–281
30. Zhang H, Schuster BE, Wei Q, Ramesh KT (2006) The design of accurate micro-compression experiments. *Scr Mater* 54:181–186
31. Uchic MD, Dimiduk DM (2005) A methodology to investigate size scale effects in crystalline plasticity using uniaxial compression testing. *Mater Sci Eng A* 400–401:268–278
32. Underwood EE (1970) Quantitative stereology. Addison-Wesley, Reading, MA
33. Maurice D, Courtney TH (1995) Modeling of mechanical alloying: Part III. Applications of computational programs. *Metall Mater Trans A* 26:2437–2444
34. Inoue A, Takeuchi A (2011) Recent development and application products of bulk glassy alloys. *Acta Mater* 59:2243–2267. doi:10.1016/j.actamat.2010.11.027
35. Chen M (2008) Mechanical behavior of metallic glasses: microscopic understanding of strength and ductility. *Annu Rev Mater Res* 38:445–469
36. Lai YH, Lee CJ, Cheng YT et al (2008) Bulk and microscale compressive behavior of a Zr-based metallic glass. *Scr Mater* 58:890–893
37. Chen CQ, Pei YT, De Hosson JTM (2010) Effects of size on the mechanical response of metallic glasses investigated through in situ TEM bending and compression experiments. *Acta Mater* 58:189–200
38. Bharathula A, Lee S-W, Wright WJ, Flores KM (2010) Compression testing of metallic glass at small length scales: effects on deformation mode and stability. *Acta Mater* 58:5789–5796
39. Jang D, Gross CT, Greer JR (2011) Effects of size on the strength and deformation mechanism in Zr-based metallic glasses. *Int J Plast* 27:858–867
40. Ke HB, Sun BA, Liu CT, Yang Y (2014) Effect of size and base-element on the jerky flow dynamics in metallic glass. *Acta Mater* 63:180–190
41. Bharathula A, Flores KM (2011) Variability in the yield strength of a metallic glass at micron and submicron length scales. *Acta Mater* 59:7199–7205
42. Wheeler JM, Raghavan R, Michler J (2012) Temperature invariant flow stress during microcompression of a Zr-based bulk metallic glass. *Scr Mater* 67:125–128
43. Wang C-C, Ding J, Cheng Y-Q et al (2012) Sample size matters for  $A_{188}Fe_7Gd_5$  metallic glass: smaller is stronger. *Acta Mater* 60:5370–5379
44. Tönnies D, Maaß R, Volkert CA (2014) Room temperature homogeneous ductility of micrometer-sized metallic glass. *Adv Mater* 26:5715–5721
45. Kuzmin OV, Pei YT, Chen CQ, De Hosson JTM (2012) Intrinsic and extrinsic size effects in the deformation of metallic glass nanopillars. *Acta Mater* 60:889–898